ELSEVIER

Journal of Alloys and Compounds 275–277 (1998) 637–641

Journal of ALLOYS AND COMPOUNDS

Hydrogen effects on the magnetic properties of $RFe_{11}Ti$ compounds

O. Isnard[a,*], S. Miraglia[a], M. Guillot[b], D. Fruchart[a]

[a]*Laboratoire de Cristallographie, CNRS, BP 166, 38042 Grenoble Cedex 9, France*
[b]*Laboratoire de Champs Magnétiques Intenses, CNRS/MPI, 38042 Grenoble, France*

Abstract

Hydrogen insertion in the $RFe_{11}Ti$ series of alloys induces a marked change in the main structural and magnetic parameters. The unit cell volume is found to increase significantly upon hydrogenation. The location of hydrogen atoms within the crystal structure is given according to neutron diffraction experiments performed on $CeFe_{11}TiH$. Magnetisation measurements have been performed on magnetically aligned samples between 4 K and 300 K in field up to 240 kOe (24 T). These high field magnetisation measurements are presented for $CeFe_{11}TiH$, $GdFe_{11}Ti$, $GdFe_{11}TiH$ and $SmFe_{11}TiH$. The room temperature saturation magnetisation is increased after hydrogen uptake. A raise of the Curie temperature upon hydrogen insertion is also observed. Among the $RFe_{11}Ti$ magnetic compounds, the $SmFe_{11}Ti$ is a potential candidate for high performance permanent magnets. © 1998 Elsevier Science S.A.

Keywords: Neutron diffraction; Magnetic properties; Hard magnets; Intermetallic compounds; Hydrides

1. Introduction

Rare-earth permanent magnets are based on alloys or compounds which are mainly composed of rare-earth elements and transition metal elements. The discovery of $Nd_2Fe_{14}B$ type of compounds initiated a search for other novel materials and the magnetic properties of iron rich rare-earth intermetallic compounds with uniaxial crystal structures have been extensively studied. In this respect, the magnetic properties of the pseudo-binary compounds with formula $RFe_{12-x}M_x$ (M=Ti,Cr,V,Al...) fulfilled some requirements dictated by the technological applications. Among these systems the RFe11Ti series has attracted considerable attention [1].

Absorption of hydrogen gas in intermetallic compounds often leads to changes in their magnetic properties [2]. During the last few years, much work has been reported concerning the R_2Fe_{17} [3] series as well as the $R_2Fe_{14}B$ one [4]. Less attention has been paid to the $RFe_{11}Ti$ series of hydrides [5–7], in particular few neutron diffraction experiments were reported and few magnetic measurements have been carried out to investigate the magneto-crystalline anisotropy of these materials. Here we present structural parameters from neutron and x-ray diffraction and high field magnetisation measurements performed in a continuous field on $CeFe_{11}Ti$ and $CeFe_{11}TiH$ as well as $SmFe_{11}TiH$.

2. Experimental details:

2.1. Sample preparation:

The alloys have been obtained by melting the starting elements in a high frequency induction furnace equipped with a water cooled copper crucible. The starting element purity was 99.99% for Fe and 99.95% for Ti and the rare-earth element. The homogeneity of the ingot was subsequently achieved by annealing at 950°C for 10 days. Prior to the annealing, the sample was wrapped in a tantalum foil and then sealed in a silica tube. The hydrogen insertion has been carried out under 20 bar of H_2 gas and thermal activation was needed to initiate the reaction. The hydrogen uptake has been determined by both gravimetric and volumetric methods. For all the studied compounds, the hydrogen content was measured to be close to one H atom per formula unit: 1.0, 0.8, 0.8 for the Ce, Gd and Sm containing compounds respectively, the estimated error bar being ± 0.1 atom per formula unit or less. For the $CeFe_{11}Ti$ compound the hydrogen content has also been confirmed by neutron diffraction. With respect to the Sm and Gd containing compounds no neutron diffraction was

*Corresponding author.

PII: S0925-8388(98)00409-5

possible due to the high absorption cross section of these nuclei. The hydrogen content was thus only measured by gravimetric and volumetric methods.

2.2. X-ray analysis

The structural parameters were derived from X-ray diffractometry. The X-ray patterns were recorded using a Guinier-Hägg focusing camera operated at Fe Kα radiation, with silicon as an internal standard. The lattice parameters have been refined, taking into account the 22 observed Bragg reflections. In order to distinguish between the easy plane and easy axis magnetocrystalline anisotropy, X-ray diffraction experiments have been performed on samples oriented under a magnetic field. For all the compounds discussed below, the X-ray patterns recorded at room temperature have evidenced an easy axis magnetocrystalline anisotropy.

2.3. Magnetic measurements

Thermomagnetic analysis of the sample, sealed in a silica tube to avoid oxidisation or hydrogen release, was performed using a home-made Faraday type balance.

Isothermal M versus H curves on magnetically aligned powder were carried out in a field up to 240 kOe at the High Field Magnet Facility in Grenoble. The extraction technique was used to measure the magnetisation in a continuous field produced by a water-cooled resistive magnet. The powder was aligned at room temperature using an orientation field of typically 10 kOe and fixed in epoxy resin. Prior to the alignment the powder was ground and then sieved leading to an average grain size of about 25 μm in diameter. The experimental accuracy is estimated to be ±4%. The anisotropy constants have been derived from the fit of the magnetisation curves recorded when applying the magnetic field parallel and perpendicular to the alignment direction of the powder. Details on the fitting procedures can be found in reference [8]. In field above 40 kOe, the magnetisation curves were found to be fitted by $M(H)=M_s+a_{H_2}$. This law of approach to saturation has been used to extract the saturation magnetisation value M_s.

2.4. Experimental of neutron diffraction

The neutron diffraction experiment has been performed at the high flux reactor of Institut Laue Langevin, using the French CRG-D1B 2 axis diffractometer. The data have been recorded with a position sensitive detector made of 400 cells covering 80 degrees of 2θ. The (311) Bragg reflection of a germanium crystal was used to monochromatise the neutron beam, leading to a wavelength of 1.286 Å. The neutron flux at the sample was about $0.4\ 10^6$ neutron $m^{-2}\ s^{-1}$. The diffraction data were analyzed using the Rietveld technique implemented in the FULLPROF program [9] allowing to determine both structural and magnetic parameters. In order to avoid the large incoherent neutron scattering of hydrogen, in the case of the sample used for neutron diffraction, deuterium was preferred to hydrogen.

3. Results and discussion

3.1. Crystal structure and neutron diffraction analysis:

The X-ray diffraction patterns show that the $RFe_{11}Ti$ as well as the $RFe_{11}TiH$ compounds retain the $I4/mmm$ symmetry. The lattice parameters determined at room temperature from X-ray diffraction analysis are summarised in Table 1. A significant increase of the unit cell is observed upon H insertion in the $CeFe_{11}Ti$, $SmFe_{11}Ti$ and $GdFe_{11}Ti$. Nevertheless this cell increase is weak in comparison with what has been reported for other intermetallic series such as R_2Fe_{17} or $R_2Fe_{14}B$ type of compounds which are known to take up larger amount of hydrogen. The percentage of volume increase is in good agreement with that found in the literature [5]. The derived volume increase per hydrogen atom is thus not constant over the series and departs from the empirical value of 2.9 $Å^3$ per hydrogen atom. The same trends is observed in the work of Zhang and Wallace [5] and seems to be common to the $RFe_{11}Ti$ compounds.

Here we focus on the analysis of the $CeFe_{11}TiH$ compound by powder neutron diffraction. The Ce compound was preferred to the Sm one because of the large absorption cross section of Sm for thermal neutron beam. The crystal structure obtained from the neutron diffraction

Table 1
Lattice and magnetic parameters of some $RFe_{11}Ti$ and $RFe_{11}TiH$ compounds

	a (Å)	c (Å)	V (Å3)	T_c (K)	K_1 (300 K) MJ m^{-3}	K_2 (300 K) MJ m^{-3}	M_s (5 K) (μ_B f.u.$^{-1}$)	M_s (300 K) (μ_B f.u.$^{-1}$)
$CeFe_{11}Ti$	8.539 (1)	4.780 (1)	348	487	1.4±0.1	−0.1±0.1	17.4±0.2	15.0±0.2
$CeFe_{11}TiH$	8.566 (1)	4.802 (1)	352	542	1.4±0.1	−0.1±0.1	17.6±0.2	15.3±0.2
$SmFe_{11}Ti$	8.568 (1)	4.798 (1)	352	567	3.9±0.2	0.1±0.1	19.4±0.2	17.5±0.2
$SmFe_{11}TiH$	8.574 (1)	4.811 (1)	354	634	4.7±0.2	0.1±0.1	19.4±0.2	18.2±0.2
$GdFe_{11}Ti$	8.536 (1)	4.792 (1)	349	621	1.5±0.1	0.1±0.1	12.7±0.2	12.0±0.2
$GdFe_{11}TiH$	8.557 (1)	4.805 (1)	352	652	1.5±0.1	0.1±0.1	13.4±0.2	12.7±0.2

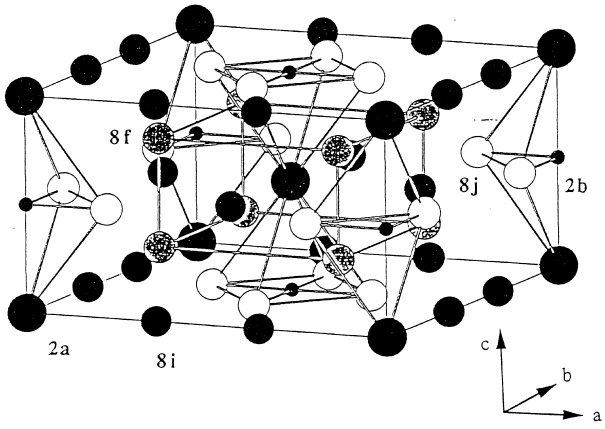

Fig. 1. Crystal structure of $CeFe_{11}TiH$ according to the neutron diffraction experiment.

experiment is shown in Fig. 1. The neutron diffraction pattern is given in Fig. 2. A small quantity of elemental iron was evidenced by neutron diffraction as an impurity. The refined amount is 4% of the total sample. The presence of such a small quantity does not alter the magnetic characterisation. It is to be noted that the presence of iron has not been detected by X-ray powder diffraction The conventional agreement factors obtained for the Rietveld analysis are the following: $R_{\text{Bragg}}=4.9\%$, $R_{\text{Weighted Profile}}=2.62\%$, $R_{\text{Magnetic}}=5.6\%$. For a definition of these parameters see reference [10]. It is found as reported in Table 2 that the Ti atoms are exclusively located in the 8*i* site of the structure. The strong affinity of Ti for this crystal site is probably mostly due to the larger Wigner-Seitz cell of the 8*i* site in comparison with sites 8*j* or 8*f* [11]. The refined Ti content: 0.96 atom/formula unit, is in good agreement with the nominal composition $CeFe_{11}Ti$ and also with the concentration deduced from

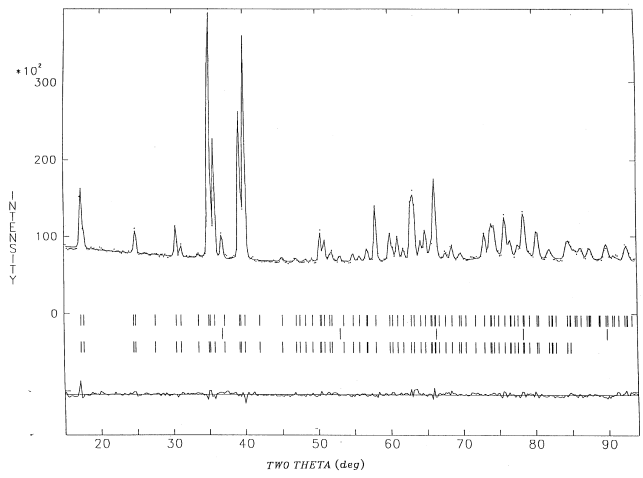

Fig. 2. Experimental (+) and calculated (continuous line) neutron diffraction pattern of $CeFe_{11}TiH$ recorded at 300 K on the D1B diffractometer. The first and third set of ticks refer to the nuclear and magnetic contribution of $CeFe_{11}TiH$ to the neutron diffraction. The second set of ticks refers to extra iron lines.

Table 2
Structural parameters obtained from neutron powder diffraction

	X	*Y*	*Z*	*B* (Å^2)	Occupancy (%)	M_z (μ_B f.u.$^{-1}$)
Ce (2*a*)	0	0	0	0.7	100	–
Fe (8*i*)	0.3534 (6)	0	0	0.7	76 (1)	1.5 (2)
Ti (8*i*)	0.3534 (6)	0	0	0.7	24 (1)	–
Fe (8*j*)	0.2753 (4)	0.5	0	0.7	100	1.5 (2)
Fe (8*f*)	0.25	0.25	0.25	0.7	100	1.5 (2)
H (2*b*)	0	0	0.5	1.9	87 (5)	–

energy dispersive X-ray analysis (EDX) implemented in our scanning electron microscope (SEM). This consistency bears witness to the good quality of the $CeFe_{11}Ti$ phase obtained.

The hydrogen concentration obtained from neutron diffraction experiment: 0.9 H atom per $CeFe_{11}Ti$ formula unit, agrees reasonably with that deduced from the gravimetric and volumetric methods (see section 'sample preparation'). This corresponds to an almost full occupancy of the interstitial 2*b* site. The hydrogen atoms are found to enter interstitial sites in the neighborhood of the rare-earth element. This interstitial site can be seen as a pseudo-octahedron with two rare-earth elements at 2.40 Å and four iron atoms 8*j* (at 1.93 Å) at the corners.

According to X-ray diffraction performed on samples oriented under a magnetic field, the magnetic moments have been constrained to be aligned along the *c* axis of the crystal structure. No magnetic moment was refined on the Ce site since X-ray spectroscopy has evidenced [12] that because Ce is in an intermediate valence state in $CeFe_{11}Ti$ and $CeFe_{11}TiH$, only a weak 4*f* contibution is expected. No magnetic moment was observed in the Ti and H atoms.

3.2. Magnetic measurements

As can be seen in Table 1, although the inserted amount of hydrogen per formula unit is weak, a pronounced increase of the Curie temperature of a few tens of degrees is observed. These $RFe_{11}Ti$ phases which derive from the $CaCu_5$ type, are known to exhibit small Fe–Fe distances which may lead to local negative exchange interactions according to the Neel-Slater curve [13]. The cell increase observed upon H insertion is at the origin of an increase of the Fe–Fe exchange interactions thus leading to the enhancement of the Curie temperature T_C. The observed raise in T_C is in agreement with earlier reported results [5,14]. We note that the Sm compound displays the largest T_C increase in spite of a rather low volume expansion. This may be due to an enhancement of the Sm–Fe contribution to the exchange interaction upon hydrogen insertion. In this $RFe_{11}Ti$ series the Sm compounds is known to exhibit a peculiar behaviour in the low temperature magnetisation curves due to the Sm sublattice, for a detailed characterisation see reference [7] and references therein.

The free energy of a single particle, i.e. a small single

crystal is given by: $E_T = K_1 \sin^2\theta + K_2 \sin^4\theta - M_s H \cos(\phi - \theta)$. Where θ is the angle between the c axis and the magnetisation M_s and ϕ is the angle between the magnetic field H and the c-axis.The first two terms represent the magnetocrystalline anisotropy for uniaxial crystals (anisotropy constants of higher order than K_2 were neglected). The K_1 and K_2 values have been extracted from fitting of the magnetisation curves.

Among the $RFe_{11}Ti$ series, the $SmFe_{11}TiH$ compound has attracted much interest. The $SmFe_{11}Ti$ is a potential candidate for high performance permanent magnet applications due to its uniaxial magnetocrystalline anisotropy combined with a rather high Curie temperature and reasonable magnetisation [15]. Insertion of hydrogen in the structure induces an increase of the Sm-sublattice magnetocrystalline anisotropy as shown in references [5,7]. The anisotropy field at room temperature is still high typically about 160 kOe. An even stronger anisotropy field is obtained at 4.2 K for $SmFe_{11}TiH$ as presented in Fig. 3. The anomaly noted for the perpendicular direction is attributed to a first order magnetisation process origin of which was discussed extensively in reference [7]. The $GdFe_{11}Ti$ compound is of interest since the Gd does not contribute to the magnetocrystalline anisotropy due to its *s* state (no orbital moment). The significant uniaxial anisotropy observed on Fig. 4 is thus only due to the Fe sublattice contribution. It is to be noted that the Fe sublattice anisotropy is not affected by insertion of hydrogen in $GdFe_{11}Ti$. The case of Ce is somewhat different since due to the strong hybridisation of the 4f and 5d electrons no 4f localised moment is present, thus, Ce should not contribute much to the magnetocrystalline anisotropy in $CeFe_{11}Ti$ and $CeFe_{11}TiH$. This hypothesis

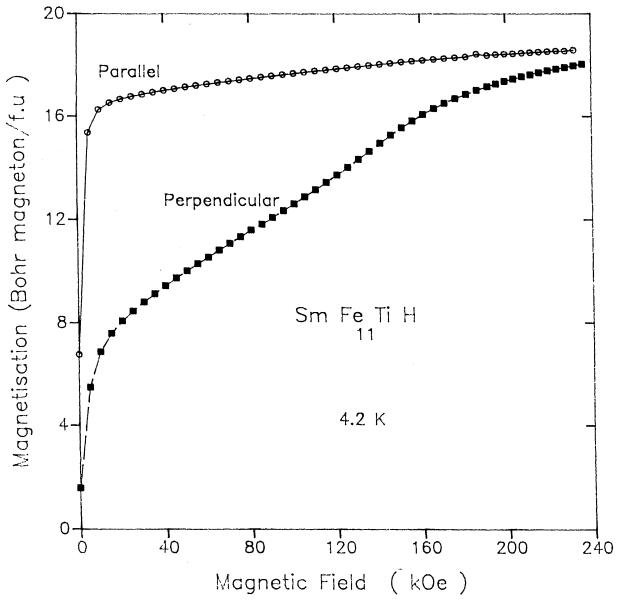

Fig. 3. Isothermal magnetisation curves at 4.2 K on oriented $SmFe_{11}TiH$ up to 240 KOe.

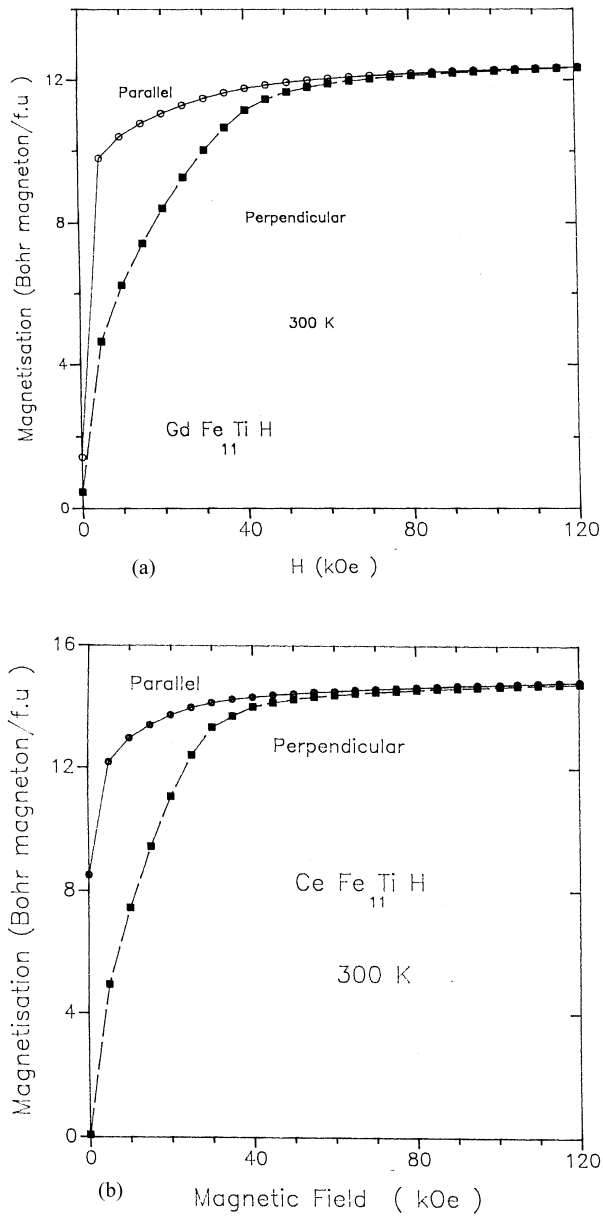

Fig. 4. Isothermal magnetisation curves at 300 K on oriented $GdFe_{11}Ti$ and $GdFe_{11}TiH$ up to 120 KOe.

seems to be confirmed by the experimental results since Ce and Gd compounds exhibit almost the same anisotropy parameters as shown in Table 1. In the case of $CeFe_{11}Ti$ as in the case of $GdFe_{11}Ti$, H insertion does not change the anisotropy parameters significantly. Comparison of the anisotropy of $SmFe_{11}TiH$ and $GdFe_{11}TiH$ evidences the strong contribution of the Sm sublattice to the magnetocrystalline anisotropy in $SmFe_{11}TiH$. Unlike what is observed for $R_2Fe_{14}B$ and R_2Fe_{17} series [8], the insertion of hydrogen in $RFe_{11}Ti$ induces an enhancement of the rare-earth contribution to the anisotropy.

In case of $CeFe_{11}TiH$ high field magnetisation curves were recorded on the oriented sample, results of which are displayed in Fig. 5. Not much change is observed upon H

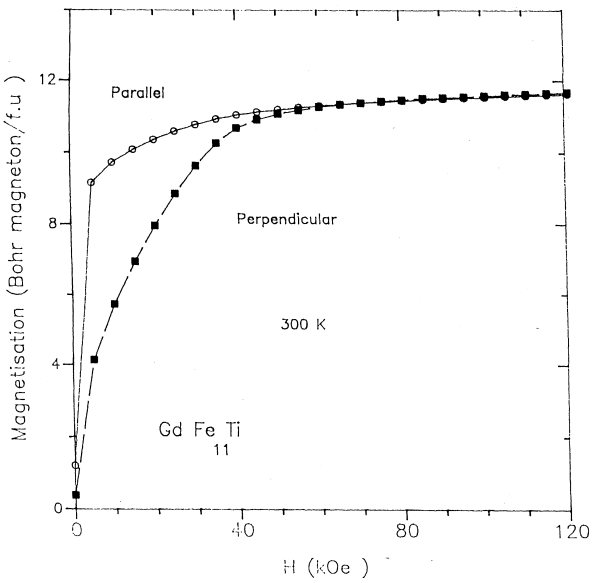

Fig. 5. Isothermal magnetisation curves at 300 K on oriented $CeFe_{11}TiH$ up to 120 KOe.

insertion neither in the anisotropy or on the saturation magnetisation corroborating the fact that Ce remains in an intermediate valence (non magnetic) state after hydrogenation.

References

[1] D.B. de Mooij, K.H.J. Buschow, J. Less Common Met. 136 (1988) 207.
[2] G. Wiesinger, G. Hilscher, in: K.H.J. Buschow (Ed.), Handbook of Magnetic Materials, vol. 6, 1991, p. 511.
[3] O. Isnard, S. Miraglia, D. Fruchart, J. Deportes, J. Magn. Magn. Mat. 103 (1992) 157.
[4] D. Fruchart, L. Pontonnier, F. Vaillant, J. Bartolome, J.M. Fernandez, K.A., Puertolas, C. Rillo, J.R. Regnard, A. Yaouanc, R. Fruchart, P. L'heritier, I.E.E.E. Trans. Magn. MAG-24, (1988) 1641.
[5] L.Y. Zhang, W.E. Wallace, J. Less Common Met. 149 (1989) 371.
[6] L.Y. Zhang, S.G. Sankar, W.E. Wallace, S.K. Malik, Proceedings of the 11th International Workshop on Rare-earth Magnets and their Applications, Pittsburgh, 1990, p. 493.
[7] O. Isnard, M. Guillot, S. Miraglia, D. Fruchart, J. Appl. Phys. 79(8) (1996) 5542.
[8] O. Isnard, S. Miraglia, M. Guillot, D. Fruchart, J. Appl. Phys. 75(10) (1994) 5988.
[9] J. Rodiguez-Carvajal, Physica B 192 (1993) 55.
[10] R.A. Young, The Rietveld Method, Oxford Univ. Press, 1993.
[11] O. Isnard, Ph. D. Thesis (1993) Universite J. Fourier, Grenoble.
[12] O. Isnard, S. Miraglia, F. Villain, Proceedings of the 9th International Conference on X-ray Absorption Fine Structure, Grenoble, 1996.
[13] L. Néel, Ann. Phys. 5 (1936) 232.
[14] L. Bozukov, A. Apostolov, M. Stoytchev, J. Magn. Magn. Mat. 101 (1991) 355.
[15] J.M.D. Coey, in G.F. Chairotti, F. Fumi, M.P. Tosi (Eds.), Current Trends in the Physics of Materials, Proceeedings of the Enrico Fermi School of Physics, Course CVI, North Holland, 1990, p. 265.